Inorganic Chemistry

Article

pubs.acs.org/IC

Computational Exploration of Alternative Catalysts for Olefin Purification: Cobalt and Copper Analogues Inspired by Nickel Bis(dithiolene) Electrocatalysis

Haixia Li,[†] Edward N. Brothers,*[,‡] and Michael B. Hall*[,†]

[†]Department of Chemistry, Texas A&M University, College Station, Texas 77843, United States

[‡]Science Program, Texas A&M University at Qatar, Education City, Doha, Qatar

Supporting Information

ABSTRACT: Olefin purification is an important process in petrochemistry. The behavior of the nickel bis(dithiolene) complex $Ni(S_2C_2(CF_3)_2)_2$ ($\mathbf{1}_{Ni}$) as an electrocatalyst for this process was thoroughly explored experimentally and computationally. Here, computational investigations with the ωB97X-D functional were conducted to explore alternative candidates $[M(S_2C_2(CF_3)_2)_2]^n$ (M = Co with n = 0, −1, −2, −3 and Cu with n = +1, 0, −1, −2) for olefin purification by using ethylene as a model. The reaction mechanism for these alternative catalysts was calculated to determine if any of these alternatives could block the decomposition route that exists for the Ni catalyst, bind ethylene efficiently to form the adducts, and release ethylene upon reduction. Calculations predict that the neutral cobalt complex $\mathbf{1}_{Co}$ binds and releases olefin upon reduction with low activation barriers. Furthermore, $\mathbf{1}_{Co}$, unlike $\mathbf{1}_{Ni}$, catalyzes the desired reaction without the need of the anion as a cocatalyst. The Co atom directly coordinates with ethylene more favorably than Ni, facilitating the indirect pathway that is found to lead to the formation of the desired interligand adduct. The reduction and oxidation processes involved in the reaction are computed to occur under reasonable experiment conditions. Among the copper complexes, the calculations predict that the anionic copper complex $\mathbf{1}_{Cu}^-$ also may be an alternative catalyst, whose performance is somewhat worse than $\mathbf{1}_{Ni}$. The reaction of $\mathbf{1}_{Cu}^-$ with ethylene is predicted to be thermodynamically neutral. New catalysts that need no electrochemical regenerations may be possible by designing appropriate dithiolene ligands for $\mathbf{1}_{Cu}^-$.

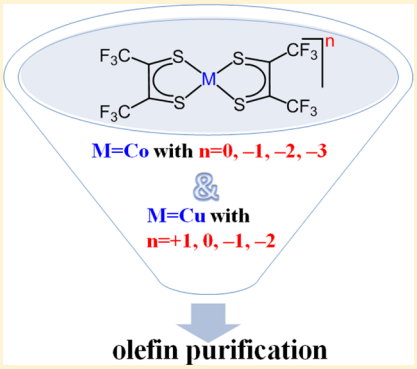

1. INTRODUCTION

Olefins are among the largest volume organic feedstock and are widely used to produce polymers, acids, alcohols, esters, and ethers.[1] General methods for producing olefins via steam or catalytic cracking and for separation by cryogenic distillation are energy-intensive and costly, contributing ~75% of the total olefin production cost.[2] Therefore, more inexpensive and efficient approaches to separating olefins from their common impurities would be useful. Redox-active metal salts such as copper react with olefin reversibly but are usually poisoned by common olefin impurities such as C_2H_2, CO, and H_2S, which impedes their applications in industry.[3] In 2001, Wang and Stiefel reported a reversible electrochemical system for olefin purification by using the nickel bis(dithiolene) complexes $Ni(S_2C_2R_2)_2$ (R = CF_3 and CN).[4] This reaction avoids the deactivation issues caused by the impurities, offering an innovative approach for olefin separation. A four-step mechanism for the catalytic reaction was proposed (Scheme 1): (1) the monoanionic complex $[NiL_2]^-$ (L = dithiolene, such as mnt ($S_2C_2(CN)_2$) or tfd ($S_2C_2(CF_3)_2$) is oxidized electrochemically to the neutral species $[NiL_2]$; (2) $[NiL_2]$ selectively binds the olefin to form the adduct $[(olefin)NiL_2]$; (3) $[(olefin)NiL_2]$ is electrochemically reduced to generate $[(olefin)NiL_2]^-$; and (4) the reduced olefin adduct $[(olefin)NiL_2]^-$ rapidly ejects olefin to regenerate $[NiL_2]^-$. In step (2), the cis-interligand adduct in which two sulfur atoms from

Scheme 1. Catalytic Cycle for Purifying Olefin with Nickel Bis(dithiolene) Complexes

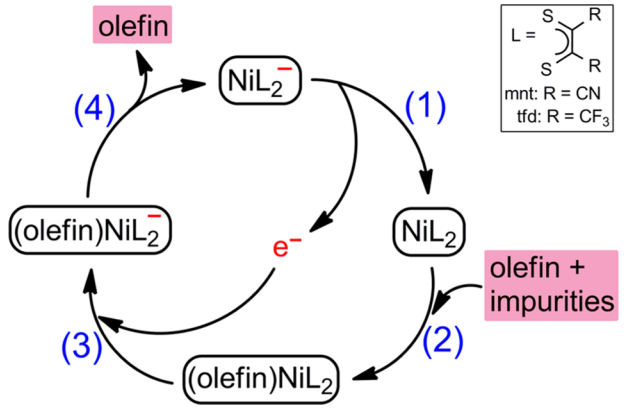

Received: May 21, 2014
Published: August 29, 2014

   dx.doi.org/10.1021/ic5011538 | Inorg. Chem. 2014, 53, 9679−9691

Scheme 2. Two-Step Mechanism Proposed for the Ethylene Binding to the Nickel Bis(dithiolene) Complexes

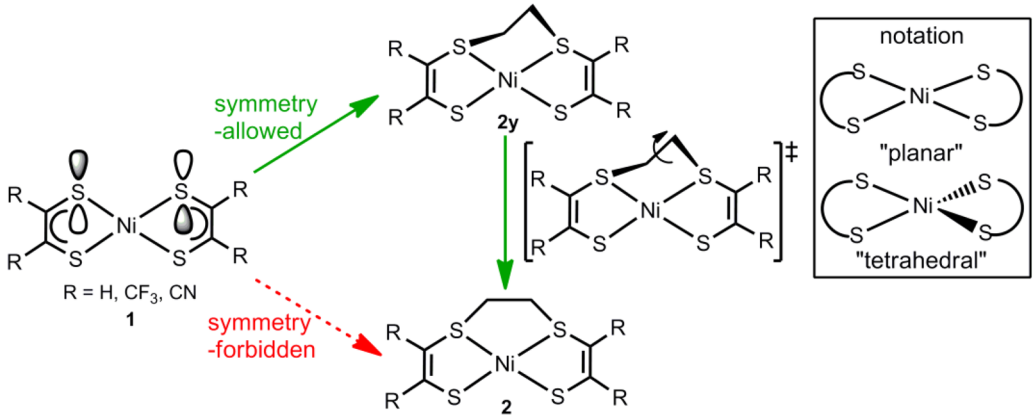

Scheme 3. Proposed Mechanism for the Reaction of $[Ni(S_2C_2(CF_3)_2)_2]$ Complex (1) with Ethylene to Produce the Intraligand Adduct 3 without 1^- and Interligand Adduct 2 with 1^-

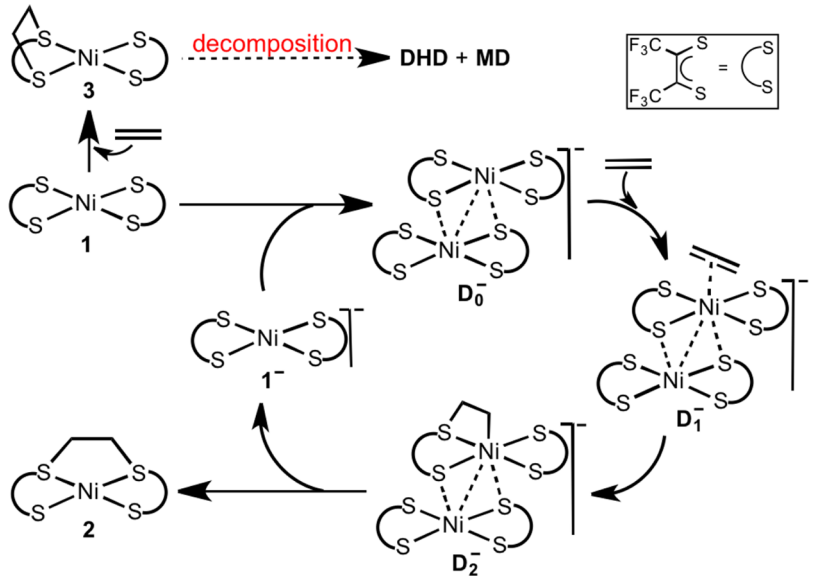

different dithiolene ligands are bridged by a new carbon–carbon bridge was thought to be formed, and similar complexes have been confirmed by X-ray crystallography.[5]

The direct formation of the cis-interligand adduct (the pathway in red in Scheme 2) violates the Woodward–Hoffmann addition rule. Therefore, a two-step mechanism (the pathway in green in Scheme 2) was proposed, which avoids the constraints imposed by orbital symmetry.[6] In this mechanism, the symmetry-allowed pathway first forms a twisted (pseudotetrahedral) adduct, which then isomerizes to the more stable square-planar cis-interligand adduct. In 2006, new experimental results showed that the two-step mechanism needs revision to explain how the one-electron-reduced form, $[Ni(S_2C_2(CF_3)_2)_2]^-$ ($[Ni(tfd)_2]^-$, $\mathbf{1}^-$), plays a crucial role in producing the interligand adduct from the reaction of $Ni(tfd)_2$ with ethylene.[5b] In the absence of $\mathbf{1}^-$, the reaction of **1** with ethylene favors the formation of the symmetry-allowed intraligand adduct **3**, which decomposes to generate the experimentally observed substituted dihydrodithiin (**DHD**) and metal decomposition (**MD**) product (top reaction in Scheme 3). A modified mechanism (the cycle in Scheme 3) was proposed through the combination of experimental and theoretical studies.[7,8] In the presence of the reduced complex $[Ni(tfd)_2]^-$ ($\mathbf{1}^-$), the desired cis-interligand adduct **2** was formed via the following process: $\mathbf{1}^-$ combines with **1** to form a dimetallic intermediate ($\mathbf{D_0}^-$), followed by the ethylene binding first to Ni (forming $\mathbf{D_1}^-$), then across the Ni–S bond giving intermediate $\mathbf{D_2}^-$, which releases $\mathbf{1}^-$ to form the complex that finally isomerizes to the cis-interligand adduct **2**.

The mechanistic studies on the reaction of $Ni(tfd)_2$ with ethylene inspired us to explore alternative catalysts for olefin purification. The ideal alternative catalysts could block the formation of the intraligand adduct (the decomposition route) and reversibly bind ethylene with lower barriers than $Ni(tfd)_2$, without the anion as the cocatalyst. Keeping these requirements in mind, we examined the related $[Co(tfd)_2]^n$ (n = 0, −1, −2, −3) and $[Cu(tfd)_2]^n$ (n = +1, 0, −1, −2) complexes and their reactions with ethylene.

2. COMPUTATIONAL METHODS

Calculations were conducted by using Gaussian 09 program.[9] Previous examinations of the simplified dithiolene $Ni(S_2C_2H_2)_2$ show that calculations with the ωB97X-D functional,[10,11] which contains both long-range exchange and empirical dispersion corrections that are very important for the modeling processes with weak interactions and localized anionic or strongly electron-donating sites, produced relative

dx.doi.org/10.1021/ic5011538 | Inorg. Chem. 2014, 53, 9679–9691

Scheme 4. Cobalt and Copper Complexes Examined in This Study

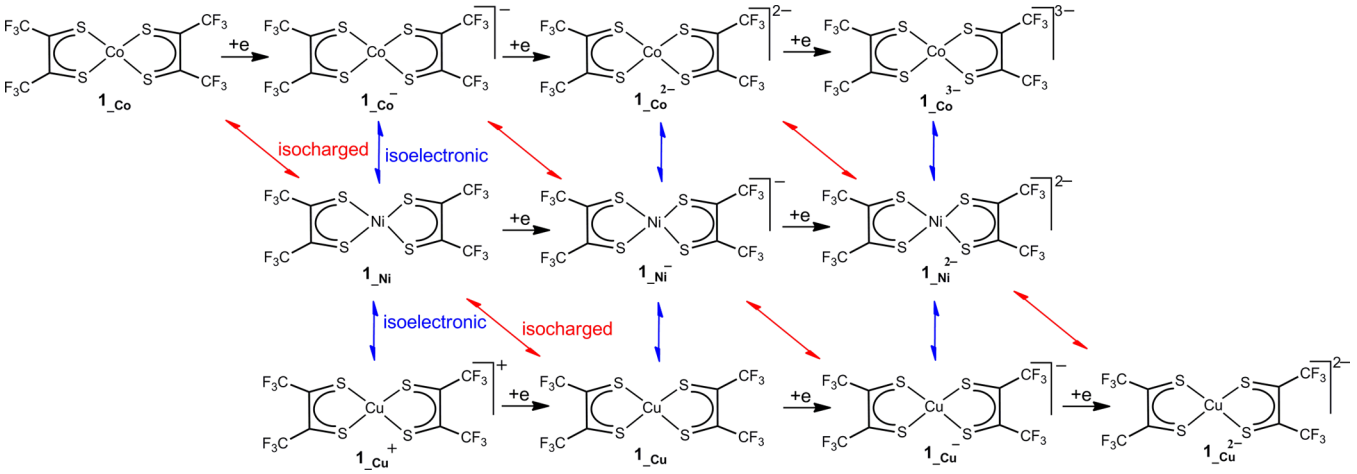

electronic energies that were similar to coupled cluster singles and doubles (CCSD) results. Therefore, geometric structures of all species in gas phase were optimized with ωB97X-D functional, and an all-electron 6-31++G(d,p) (5d) Pople basis set was specified for all the atoms.[12] A key word of "ultrafine" with a pruned (99 590) grid was used to optimize larger molecules with many soft modes such as methyl rotations, making such optimizations more reliable. Harmonic vibrational frequencies were calculated to identify intermediates with no imaginary frequencies and transition states with only one imaginary frequency. Transition states were checked to be sure that they connect the two corresponding intermediates before and after them by the vibration mode of the imaginary frequency. Intrinsic reaction coordinate (IRC) calculations were further conducted when necessary.[13]

Calculations were carried out to test the stability of the density functional theory wave functions.[14] For the open shell calculations, $\langle S^2\rangle$ values were also checked, and we adopted the formula, which is deduced from the Yamaguchi broken-spin-symmetry procedure,[15] to compute the energy of the spin-purified low-spin state (^{LS}E) from the calculated energies of the broken symmetry solution (^{BS}E) and the high-spin coupled state (^{HS}E) that is related to single-determinantal broken spin-symmetry state by a simple spin-flip. The corrected energies are reported in the manuscript, and uncorrected energies together with the corresponding $\langle S^2\rangle$ values are in the Supporting Information.

$$^{LS}E = \frac{^{BS}E(^{HS}\langle S^2\rangle - ^{LS}\langle S^2\rangle) - ^{HS}E(^{BS}\langle S^2\rangle - ^{LS}\langle S^2\rangle)}{^{HS}\langle S^2\rangle - ^{BS}\langle S^2\rangle}$$

The solvation effects with chloroform as solvent were taken into account by doing single-point calculations based on the gas-phase optimized geometries. The ωB97X-D functional and all-electron 6-31++G(d,p) (5d) basis set with the solvation model density (SMD) method were used in the simulations.[16] The harmonic frequencies obtained by the gas-phase optimizations were used for the thermal and entropic corrections to the enthalpies and free energies at 298.15 K. The solvation corrected free energies will be reported in the discussions, unless otherwise specified. The di- and trianionic species were optimized in solution at the level of ωB97X-D/6-31++G(d,p) (5d) with SMD solvent model, because the solvation parameters can prevent the delocalization of the negative charge from forming an inaccurate Rydberg-like state that could occur in gas-phase optimizations.[17] The gas-phase optimizations of the monoanionic species have reasonable structures and are similar to those obtained from the optimization in solvent (see the Supporting Information); likewise, the energies and trends from single-point solvent corrections of the gas-phase geometries are unaltered from those optimized in solvent (see the Supporting Information). Minimum energy crossing points (MECP) were calculated with the MECP program of Harvey and co-workers.[18] The three-dimensional molecular geometries were drawn by using the JIMP2 visualization program.[19]

3. RESULTS AND DISCUSSION

The noninnocent character of the dithiolene ligand makes it difficult to assign the oxidation state of the metal center for the metal bis(dithiolene) complexes.[20] The electronic structure of the neutral nickel bis(dithiolene) complex has been widely studied both experimentally and theoretically, elucidating that the best description of their oxidation state is Ni^{II}.[21,22] Furthermore, investigations have identified the existence of the reversible one-electron redox series $[Ni(S_2C_2(CF_3)_2)_2]$ ($\mathbf{1}_{Ni}$) ↔ $[Ni(S_2C_2(CF_3)_2)_2]^-$ ($\mathbf{1}_{Ni}^-$) ↔ $[Ni(S_2C_2(CF_3)_2)_2]^{2-}$ ($\mathbf{1}_{Ni}^{2-}$) (Scheme 4) in which the electrons are added and removed from the bis(dithiolene) systems and the Ni remains Ni^{II}.[23] With redox noninnocent ligands, it is not obvious what electron counts on other metals would promote the desired reaction. Therefore, the cobalt and copper bis(dithiolene) complexes that are both isoelectronic and isocharged to the three forms of the nickel bis(dithiolene) complexes were chosen (Scheme 4). As in the previous study, the dithiolene ligand for the cobalt and copper complexes was the CF_3-substituted system (tfd). The pre-superscript, when present on the symbols, indicates a particular spin state of the complex, and the overall charge is shown in the superscript on the metal; for example, $^2\mathbf{1}_{Ni}^-$ denotes the doublet complex of the nickel bis(dithiolene) anion.

The anionic cobalt complexes $^1\mathbf{1}_{Co}^-$ and $^3\mathbf{1}_{Co}^-$ and the cationic copper complexes $^1\mathbf{1}_{Cu}^+$ and $^3\mathbf{1}_{Cu}^+$ are isoelectronic to the reported neutral nickel complex $^1\mathbf{1}_{Ni}$. Molecular orbital (MO) analyses of their singlet-state planar geometries (see the Supporting Information) show that they have similar MOs in somewhat different sequences. Thus, both $^1\mathbf{1}_{Co}^-$ and $^1\mathbf{1}_{Cu}^+$ have electronic structures that appear to be well-described as low-spin, d^8 metals (Co^I and Cu^{III}, respectively) with monoanionic ligands, $[S_2C_2(CF_3)_2]^-$, (the pair delocalized by direct coupling into a singlet) like $^1\mathbf{1}_{Ni}$. However, the lowest energy structure for $\mathbf{1}_{Cu}^+$ is the tetrahedral singlet $^1\mathbf{1}_{Cu}^+$, in which case the ligands become more dithiolene-like (less anionic with more neutral $S_2C_2(CF_3)_2$ character), and the Cu moves closer to being d^{10} Cu^I, while the lowest energy structure for $\mathbf{1}_{Co}^-$ is the square planar triplet $^3\mathbf{1}_{Co}^-$, in which case the ligands become more dithiolate-like (more anionic; upon the spin change the paired electrons move to the ligand framework,

dx.doi.org/10.1021/ic5011538 | Inorg. Chem. 2014, 53, 9679−9691

while the two excess "α" electrons move to the metal), and the Co appears like intermediate-spin d^6 Co^{III}. Because of the noninnocent nature of these "dithiolene" ligands, high-spin or odd electron species are even more difficult to analyze, and assignment of definitive oxidation states are impossible.

Overall, a good alternative catalyst should block the decomposition route that involves the intraligand adduct **3**, bind ethylene through the interligand adduct **2**, and release ethylene upon reduction. The thermodynamics for the formations of the interligand adduct, **2**, or its twisted isomer, **2y**, and the intraligand adduct, **3**, are presented briefly in Section 3.1. Additionally, a good alternative catalyst should have low activation barriers and form **2** without the presence of the anion. The barriers for the reactions of ethylene with cobalt and copper complexes that are selected from Section 3.1 (the complexes that have passed through the thermodynamics requirements) are presented in Sections 3.2 and 3.3, respectively.

3.1. Thermodynamics Results for the Reactions of Cobalt or Copper Bis(dithiolene) Complexes with Ethylene. Calculated thermodynamic results for the cobalt or copper bis(dithiolene) complexes together with the nickel complexes are summarized in Table 1. Two spin states, the lowest spin state and the next higher spin state, were calculated for each complex. Although both experimental and computational studies show that the nickel bis(dithiolene) complex adopts a planar geometry,[21,22] geometric searches were made for a tetrahedral structure in addition to the planar one. The most stable form of each metal bis(dithiolene) complex was considered the reference minimum for the estimation of the free energies calculated here.

Table 1. Calculated Thermodynamics for the Nickel, Cobalt, and Copper Complexes

complex	planar	tetrahedral	2y	2	3
^{1}**1**$_{Ni}$	0.0	*a*	−16.1	−17.8	−14.8
^{3}**1**$_{Ni}$	0.9	*a*	−21.8	−14.7	−5.7
^{2}**1**$_{Ni}^-$	0.0	*a*	13.9	18.9	26.8
^{4}**1**$_{Ni}^-$	*b*	15.3	43.2	51.3	35.1
^{1}**1**$_{Ni}^{2-}$	0.0	*a*	73.0	88.6	58.0
^{3}**1**$_{Ni}^{2-}$	0.6	*a*	60.5	65.7	52.1
^{2}**1**$_{Co}$	0.0[c]	*b*	−22.3	−25.6	−13.3[d]
^{4}**1**$_{Co}$	0.4	*b*	−31.1	−25.7	−23.0[e]
^{1}**1**$_{Co}^-$	14.0[f]	9.0[f]	40.0[f]	41.6[f]	48.1[f]
^{3}**1**$_{Co}^-$	0.0	*a*	16.4	25.9	31.2
^{2}**1**$_{Co}^{2-}$	5.0	*a*	82.0[c]	90.9	69.9[c]
^{4}**1**$_{Co}^{2-}$	*a*	0.0	63.6	92.3	60.2
^{1}**1**$_{Co}^{3-}$	0.0	*a*	*g*	*g*	*g*
^{3}**1**$_{Co}^{3-}$	28.6	*b*	*g*	71.2	89.0[c]
^{1}**1**$_{Cu}^+$	11.2	0.0	−25.6	−27.5	−31.7
^{3}**1**$_{Cu}^+$	4.6	*a*	−26.4	−25.4	−43.4
^{2}**1**$_{Cu}$	0.0[c,h]	*a*	−22.0	−22.2	−24.6[e]
^{4}**1**$_{Cu}$	0.6[h]	*a*	18.7	18.6	15.2[e]
^{1}**1**$_{Cu}^-$	0.0	*a*	−9.5	−3.3	−1.5[e]
^{3}**1**$_{Cu}^-$	3.0	5.0	25.5	39.8	26.4
^{2}**1**$_{Cu}^{2-}$	0.0	*a*	42.5	43.0	31.3
^{4}**1**$_{Cu}^{2-}$	39.2	*a*	77.7	77.0	66.7

[a]The geometry optimization converged to other isomers. [b]The geometry optimization failed to converge. [c]The values after correction by using Yamaguchi procedure. [d]The wave function has internal instability. [e]Structure optimizations give the tetrahedral geometry, and ^{1}**3**$_{Cu}^-$ has three sulfur atoms coordinate to copper atom. [f]The wave function has RHF > UHF instability. [g]The optimizations result in F atom dissociation. [h]The geometry is not exactly planar; the ligands are slightly twisted.

Results for the reaction of neutral nickel bis(dithiolene) complex with ethylene in Table 1 show that the triplet state of the twisted interligand adduct ^{3}**2y**$_{Ni}$ is the most stable one among possible adducts. However, the cis-interligand adduct ^{1}**2**$_{Ni}$ was observed in experiment as the stable final product.[5b] One possible explanation for the inconsistency between the computational and experimental results is that the ωB97X-D functional may overestimate the energy gap of high-spin state (HS) and low-spin state (LS), favoring the high-spin state. To verify this and further estimate the computed errors for the HS−LS gaps, more accurate CCSD(T) calculations were conducted by using the simplified model, $Ni(edt)_2$ (edt = $S_2C_2H_2$) (see the Supporting Information). The cis-interligand adduct ^{1}**2**$_{Ni\_model}$ is more stable than the twisted interligand adduct ^{3}**2y**$_{Ni\_model}$ by 1.7 kcal/mol (electronic energy) at the level of CCSD(T)/6-31++G(d,p), a result consistent with the experimental observations. ^{1}**2**$_{Ni\_model}$ is also more stable than ^{3}**2y**$_{Ni\_model}$ by 2.0 kcal/mol (electronic energy) at the level of M06/6-31++G(d,p), producing a result very close to that from CCSD(T). In contrast, the ^{1}**2**$_{Ni\_model}$ adduct is less stable than the ^{3}**2y**$_{Ni\_model}$ adduct by 4.5 kcal/mol (electronic energy) at the level of ωB97X-D/6-31++G(d,p). The comparisons show that the ωB97X-D functional underestimates the HS−LS gaps by at least 6 kcal/mol for the simple $Ni(edt)_2$ system. Although this gives us an estimation of possible errors in comparions of spin-state energies, the unpaired electrons in this example are on Ni, while that is not the case for every species. Therefore, caution should be exercised when using this estimate. The reduced adducts **2y**$_{Ni}^{-/2-}$, **2**$_{Ni}^{-/2-}$, and **3**$_{Ni}^{-/2-}$ are all higher in energy than the separate **1**$_{Ni}^{-/2-}$ and ethylene, results consistent with the experimental observations that ethylene can be released upon reduction.

Results for the cobalt bis(dithiolene) complexes in Table 1 show that the neutral complexes (^{2}**1**$_{Co}$ and ^{4}**1**$_{Co}$) prefer a planar geometry and that the doublet-state complex ^{2}**1**$_{Co}$ is more stable than the quartet-state complex ^{4}**1**$_{Co}$ by 0.4 kcal/mol. In contrast, the ethylene adducts prefer the quartet state, and ^{4}**2y**$_{Co}$ is the most stable among them. The stability of this high-spin state (quartet state here) is likely overestimated, but the doublet-state complex ^{2}**2**$_{Co}$ is more stable than ^{2}**3**$_{Co}$ by 12.3 kcal/mol, a much larger difference than that in Ni systems. Therefore, the thermodynamics are favorable for the neutral cobalt bis(dithiolene) complex as an alternative catalyst. The one-electron reduced cobalt complex and its ethylene adducts all favor the triplet state by about 14 to 24 kcal/mol. In addition, the stability calculations show that all the singlet species have wave functions showing restricted Hartree−Fock > unrestricted Hartree−Fock (RHF > UHF) instability. The ethylene adducts ^{3}**2y**$_{Co}^-$, ^{3}**2**$_{Co}^-$, and ^{3}**3**$_{Co}^-$ are all higher in energy than the separated ^{3}**1**$_{Co}^-$ and ethylene, indicating that ethylene can be released from these adducts. In contrast to the neutral, one-electron, and three-electron reduced cobalt complexes that favor planar geometries, the two-electron reduced cobalt complex ^{4}**1**$_{Co}^{2-}$ favors a tetrahedral geometry. For all ethylene adducts of the reduced Co complexes, ethylene additions are thermodynamically very unfavorable, which can be ascribed to the fact that ethylene is a nucleophile in this

dx.doi.org/10.1021/ic5011538 | Inorg. Chem. 2014, 53, 9679−9691

process. Therefore, the more negative charge on the complex, the more difficult it is to bind the ethylene to the complex.

Results for the copper complexes in Table 1 show that the cationic copper complex $^{1}\mathbf{1}_{Cu}^{+}$, isoelectronic to the neutral Ni complex $^{1}\mathbf{1}_{Ni}$, favors the singlet state with a tetrahedral geometry. Addition of ethylene to the cationic copper complex ($^{1}\mathbf{1}_{Cu}^{+}$ and $^{3}\mathbf{1}_{Cu}^{+}$) is thermodynamically favorable by more than 25 kcal/mol energy. The neutral copper complex prefers the doublet planar structure $^{2}\mathbf{1}_{Cu}$ and also binds ethylene favorably. The one-electron reduced copper complex favors a singlet-state planar geometry, namely, $^{1}\mathbf{1}_{Cu}^{-}$. Its ethylene adducts also favor the singlet state, and the twisted interligand adduct $^{1}\mathbf{2y}_{Cu}^{-}$ is most stable. Thus, among the copper complexes, the anionic species $^{1}\mathbf{1}_{Cu}^{-}$ may be an alternative catalyst, because it binds ethylene nearly reversibly. Upon reduction, the thermodynamics for the ethylene release are favorable, because the reduced adducts $\mathbf{2y}_{Cu}^{2-}$, $\mathbf{2}_{Cu}^{2-}$, and $\mathbf{3}_{Cu}^{2-}$ are very high in energy relative to the separated $\mathbf{1}_{Cu}^{2-}$ and ethylene. Comparisons show that the cationic copper complex can be excluded due to the difficult release of ethylene from its reduced adducts, the neutral species $^{2}\mathbf{2y}_{Cu}$, $^{2}\mathbf{2}_{Cu}$, and $^{2}\mathbf{3}_{Cu}$. The neutral copper complex $^{2}\mathbf{1}_{Cu}$ might be an alternative catalyst if the thermodynamically favorable intraligand adduct $^{2}\mathbf{3}_{Cu}$ does not decompose, and this issue will be checked subsequently in Section 3.3.

The thermodynamics results in Table 1 show that the ethylene binding energies are highest (most stable) for the cationic copper complexes, followed by the neutral nickel complex, and then the anionic cobalt complexes. The following two points can explicate their different reactivity with ethylene. As mentioned above, ethylene acts as a nucleophile in the reaction, so its addition to the positively charged species, the cationic copper complexes, is more favorable than its addition to the neutral nickel complex, while its addition to the anionic cobalt complexes is even more unfavorable than its addition to the nickel complex. The other explanation is related but focuses on the frontier molecular orbitals (FMO). The FMOs of these species in Table 2 are consistent with their binding abilities to ethylene. The energy difference between the complexes' LUMOs, which are quite similar in character for all three complexes, and ethylene's HOMO (ΔE) increases through the sequence of cationic copper complex, neutral nickel complex, and anionic cobalt complex. Therefore, their binding abilities to ethylene become more and more difficult by following this sequence. The cobalt complex $^{2}\mathbf{1}_{Co}$ and the copper complex $^{2}\mathbf{1}_{Cu}$ are isocharged to $^{1}\mathbf{1}_{Ni}$. The thermodynamics for their reactivity with ethylene are not so different, differing by less than 7.8 kcal/mol. Their MOs (see the Supporting Information) are similar, and their FMO energies are close (see Table 2).

Table 2

complex[a]	HOMO[b]	LUMO[b]	ΔE[c]
C_2H_4	−9.50	2.58	
$^{1}\mathbf{1}_{Ni}$	−8.76	−3.54	5.96
$^{2}\mathbf{1}_{Co}$	−8.62(−9.07)	−3.79(−1.77)	5.71(7.73)
$^{1}\mathbf{1}_{Co}^{-}$	−7.53	−0.85	8.65
$^{1}\mathbf{1}_{Cu}^{+}$	−10.15	−5.69	3.81
$^{2}\mathbf{1}_{Cu}$	−8.51(−8.81)	−3.14(−3.25)	6.36(6.25)

[a]The nickel, cobalt, and copper complexes in this table adopt planar geometries; for $^{2}\mathbf{1}_{Co}$ and $^{2}\mathbf{1}_{Cu}$, values outside and inside the parentheses are the αMOs and βMOs, respectively. Note that a small basis set (vs the energy calculations) was used here to produce valence-like LUMOs. [b]Frontier MOs energies of C_2H_4, $^{1}\mathbf{1}_{Ni}$, $^{2}\mathbf{1}_{Co}$, $^{1}\mathbf{1}_{Co}^{-}$, $^{1}\mathbf{1}_{Cu}^{+}$, and $^{2}\mathbf{1}_{Cu}$ complexes. [c]The energy difference between the LUMO of the complex and the HOMO of C_2H_4 = ΔE. Energies (eV) are solvent-corrected MO energies at the level of ωB97X-D/6-31G(d,p).

3.2. Transition States for the Reaction of Cobalt Bis(dithiolene) Complexes with Ethylene. The thermodynamics for the reaction of cobalt bis(dithiolene) complexes with ethylene (Section 3.1) suggest that the neutral species ($^{2}\mathbf{1}_{Co}$ and $^{4}\mathbf{1}_{Co}$) might be alternative catalysts. The kinetic feasibility of this possibility is studied by locating intermediates and transition states involved in the reaction pathways. The previous mechanistic investigations for the reaction of $^{1}\mathbf{1}_{Ni}$ with ethylene show that two pathways are possible. In one, ethylene adds directly to the two sulfur atoms of either the same ligand or different ligands, generating the intraligand and interligand adducts, respectively. In the other one, ethylene first adds across the Ni−S bond, followed by isomerizations to the intraligand and interligand adducts, respectively.[24] We refer to the former pathway as the "direct" pathway and to the latter one as the "indirect" pathway. Both doublet and quartet energy surfaces for the reaction of ethylene with $^{2}\mathbf{1}_{Co}$ and $^{4}\mathbf{1}_{Co}$ were investigated and are reported in this section.

Figure 1 shows the doublet energy surfaces for the reaction of $^{2}\mathbf{1}_{Co}$ with ethylene, the dotted and solid lines denoting the direct and indirect pathways, respectively. Figure 2 shows the optimized geometries of selected intermediates and transition states involved in Figure 1. Along the direct pathway (dotted pathway in Figure 1), the cis-interligand adduct $^{2}\mathbf{2}_{Co}$ is formed by overcoming an activation barrier of 18.1 kcal/mol for $^{2}\mathbf{TS}_{2y\_Co}$ to form the twisted interligand adduct $^{2}\mathbf{2y}_{Co}$, followed by isomerization to give $^{2}\mathbf{2}_{Co}$ through an activation barrier of 15.7 kcal/mol relative to $^{2}\mathbf{2y}_{Co}$. Alternatively, ethylene can bind two sulfur atoms of the same ligand directly by crossing transition state $^{2}\mathbf{TS}_{3\_Co}$, with an activation barrier of 16.1 kcal/mol, to form the intraligand adduct $^{2}\mathbf{3}_{Co}$. The stability analysis of $^{2}\mathbf{3}_{Co}$ shows that its wave function has internal instability. Consequently, the quartet state complex $^{4}\mathbf{3}_{Co}$ is more stable than $^{2}\mathbf{3}_{Co}$ by 9.7 kcal/mol (see Figure 3 and the following discussions). Thus, the more kinetically favorable direct pathway for the reaction of $^{2}\mathbf{1}_{Co}$ and ethylene would lead to the intraligand isomer, which would likely lead to decomposition as it does for the nickel complex. For the optimized geometry of $^{2}\mathbf{1}_{Co}$ in Figure 2, the C−S and C−C bond lengths of the two ligands are between the single bond and double bond, showing the delocalized character of the ligands. Optimized geometries of $^{2}\mathbf{2y}_{Co}$, $^{2}\mathbf{2}_{Co}$, and $^{2}\mathbf{3}_{Co}$ have notable C═C bonds in the ligands and have two anionic sulfur atoms coordinate with the Co metal. Therefore, the oxidation state of Co is Co^{II} for each complex. The atomic spin densities for the Co atom of $^{2}\mathbf{1}_{Co}$ is −1.0, and that for each sulfur atom is ∼0.4, indicating that there is one β spin on the Co atom and one α spin on each ligand. Thus, the Co^{II} has its unpaired electron antiferromagnetically coupled to the ligands in their radical form. In contrast, the atomic spin densities localize on the Co atoms for the ethylene adducts $^{2}\mathbf{2y}_{Co}$, $^{2}\mathbf{2}_{Co}$, and $^{2}\mathbf{3}_{Co}$, consistent with effectively closed shell ligands (one neutral, one dianionic), and the net spin is α on the Co.

The alternative indirect pathway (solid pathway in Figure 1) involves first the formation of an intermediate $^{2}\mathbf{4}_{Co}$ in which ethylene coordinates with the Co atom. $^{2}\mathbf{4}_{Co}$ is −11.0 kcal/mol

dx.doi.org/10.1021/ic5011538 | Inorg. Chem. 2014, 53, 9679−9691

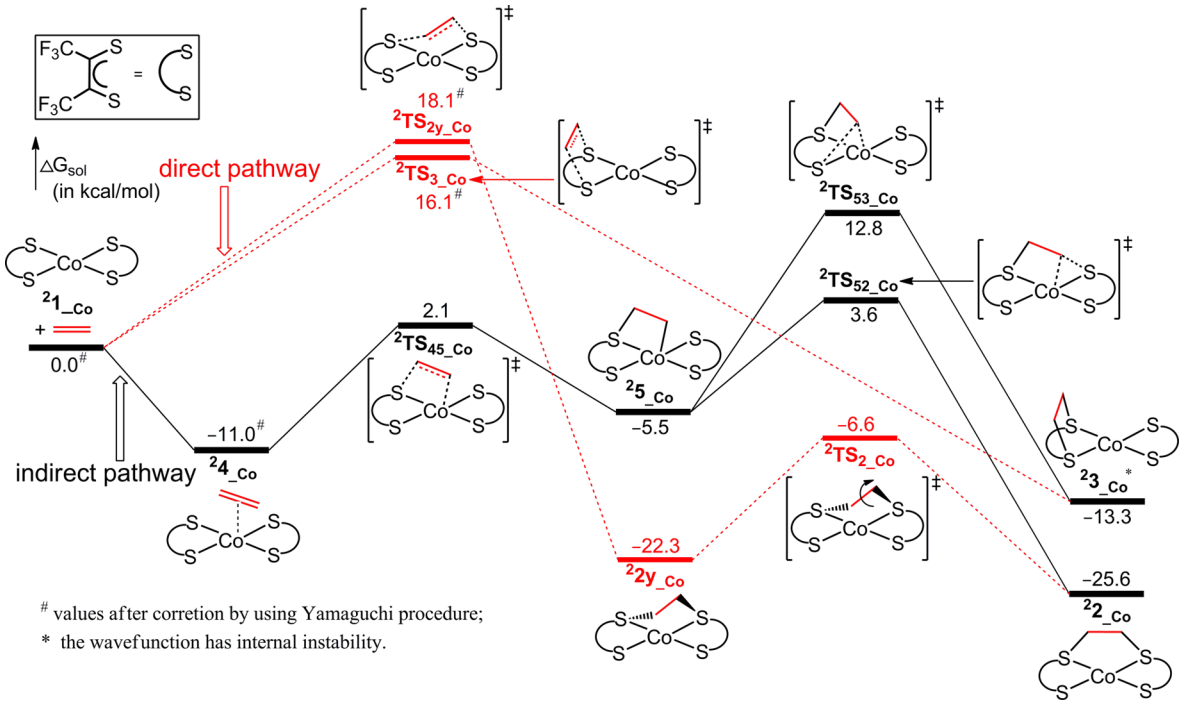

Figure 1. Calculated energy surfaces for the reaction of $^{2}\mathbf{1}_{\_Co}$ with ethylene via the direct pathway (dotted lines) or the indirect pathway (solid lines). Energies in kcal/mol are the free energy in solvent.

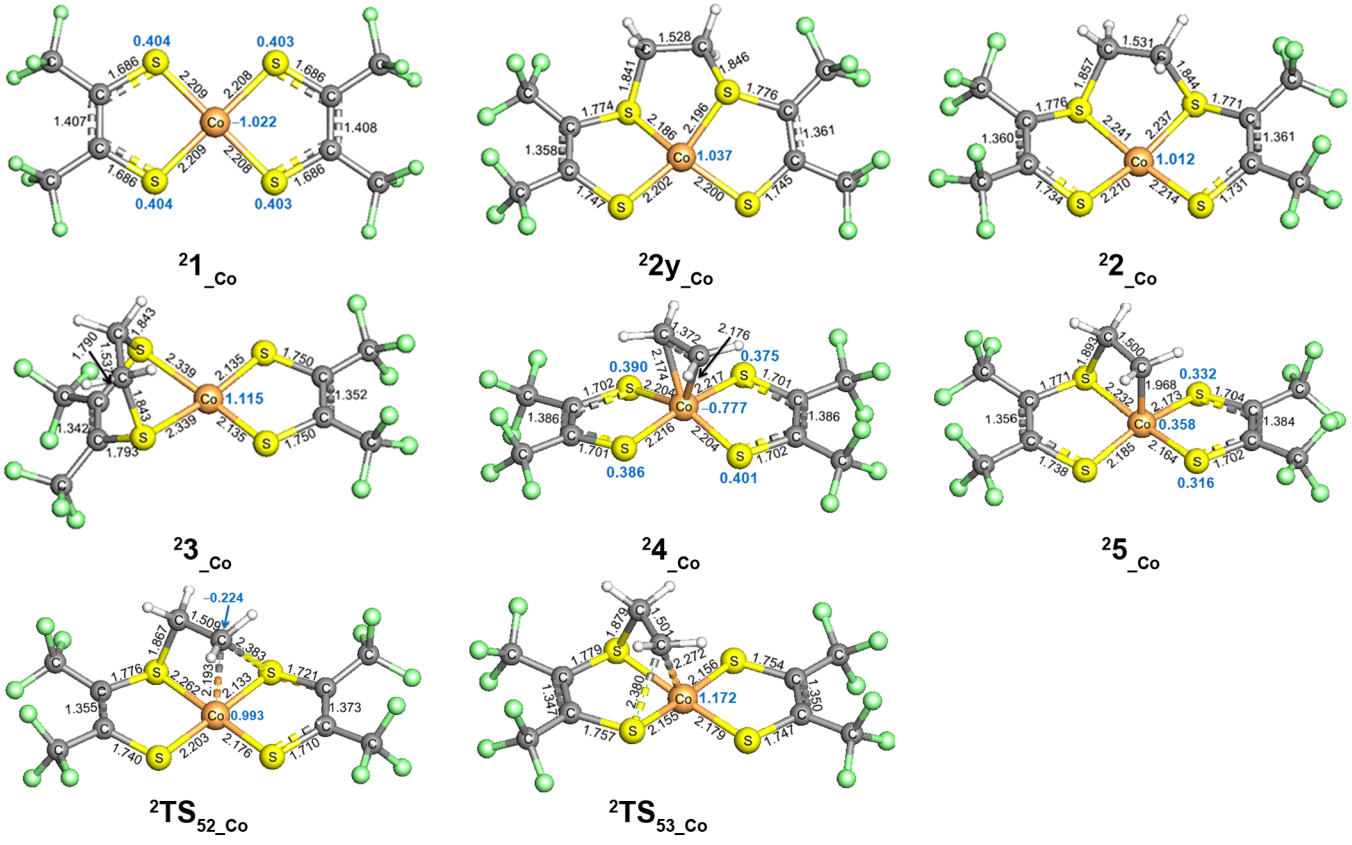

Figure 2. Optimized geometries for selected intermediates and transition states involved in Figure 1. Values in black and blue are the bond length (in Å) and the atomic spin densities, respectively. The other optimized geometries are in the Supporting Information.

relative to the separate $^{2}\mathbf{1}_{\_Co}$ and ethylene. Optimized geometry of $^{2}\mathbf{4}_{\_Co}$ shows that there are two weak Co−C interactions with lengths of 2.176 and 2.174 Å, respectively, implying that it is an η^2-coordination complex. The atomic spin densities localizations of $^{2}\mathbf{4}_{\_Co}$ are similar to those of $^{2}\mathbf{1}_{\_Co}$. In contrast, ethylene binding in the corresponding nickel complex $^{1}\mathbf{4}_{\_Ni}$ is

dx.doi.org/10.1021/ic5011538 | Inorg. Chem. 2014, 53, 9679−9691

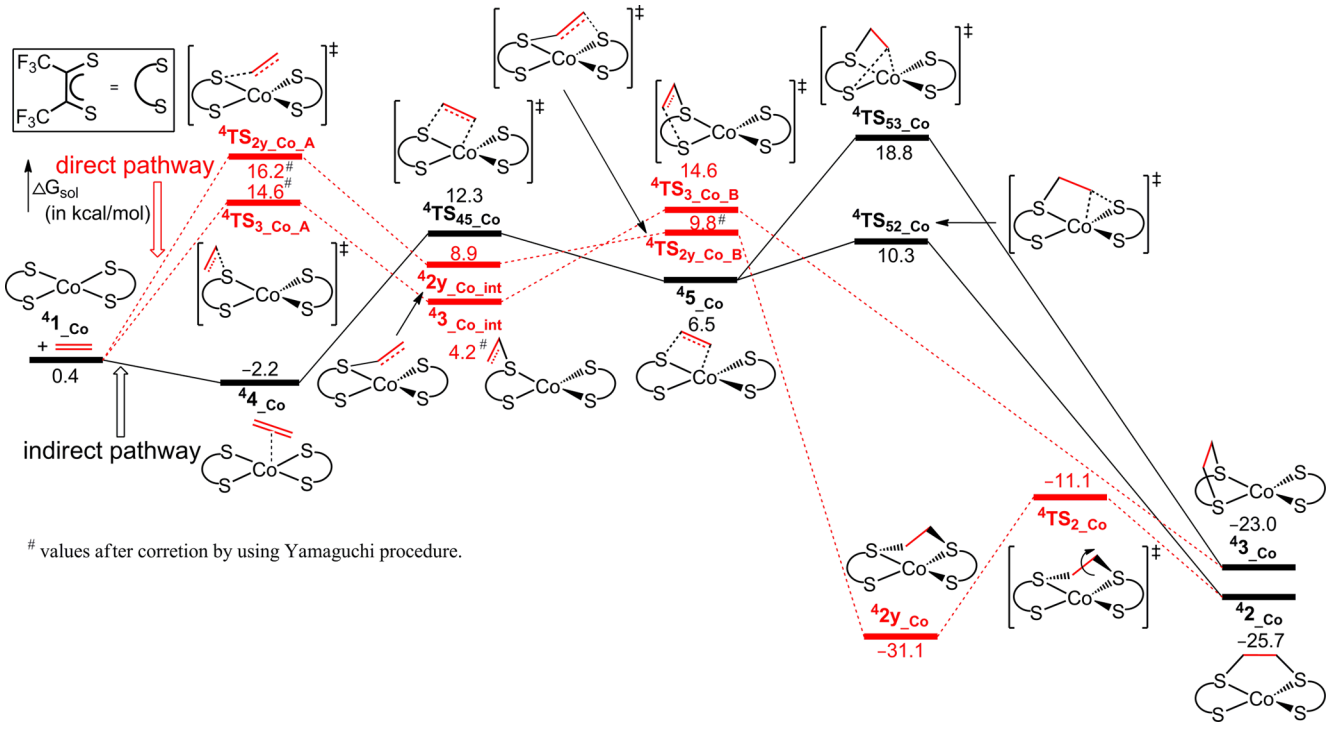

Figure 3. Calculated energy surfaces for the reaction of $^{4}\mathbf{1}_{\_Co}$ with ethylene via the direct pathway (dotted lines) or the indirect pathway (solid lines). Energies in kcal/mol are the free energy in solvent.

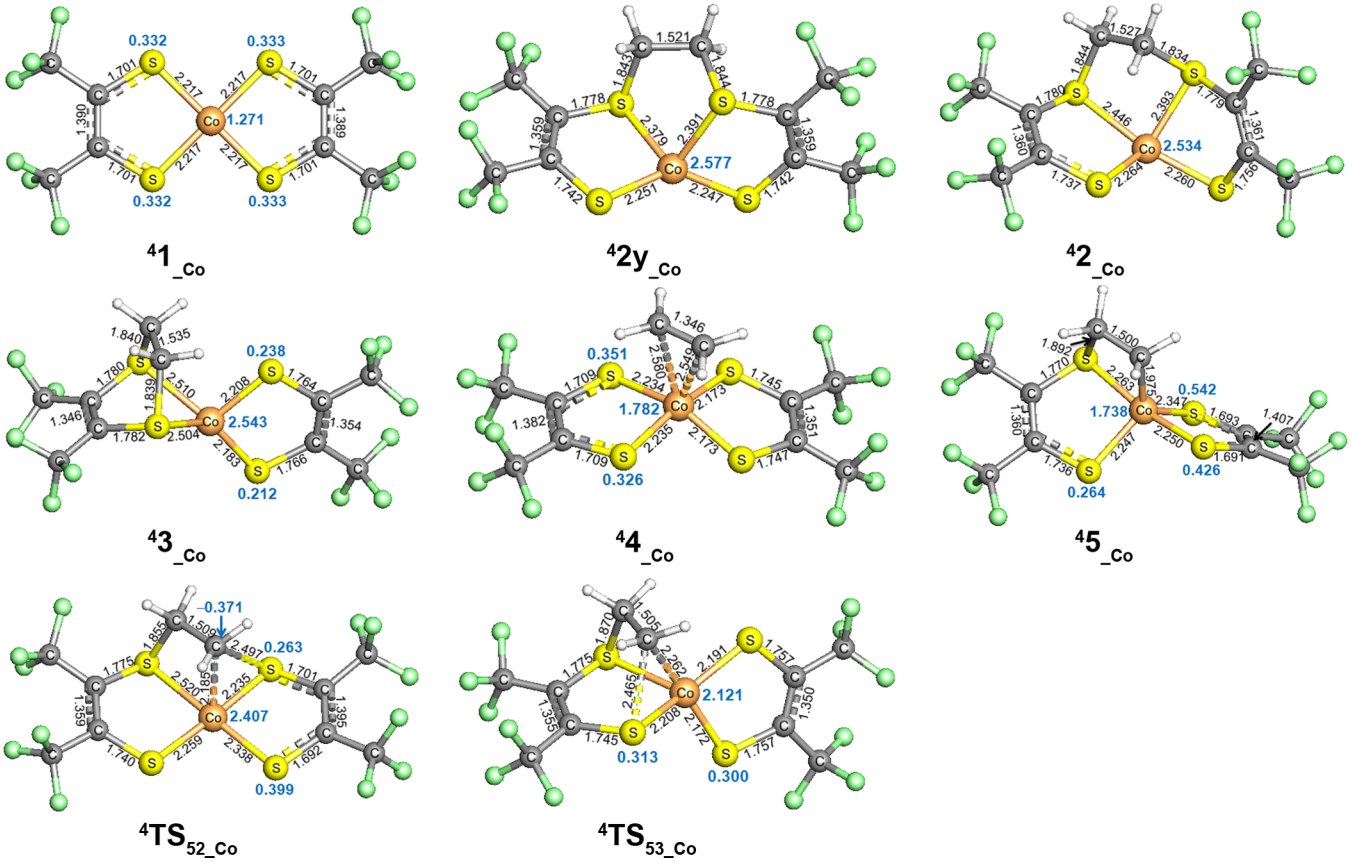

Figure 4. Optimized geometries for selected intermediates and transition states involved in Figure 3. Values in black and blue are the bond length (in Å) and the atomic spin densities, respectively. The other optimized geometries are in the Supporting Information.

very weak, as it is 20.4 kcal/mol above the separate $^{1}\mathbf{1}_{\_Ni}$ and ethylene (due to the four electron (e^{-}) repulsive interactions between them).[7,8] Subsequently, ethylene adds across the Co–S bond to generate another intermdiate $^{2}\mathbf{5}_{\_Co}$ by overcoming an

dx.doi.org/10.1021/ic5011538 | Inorg. Chem. 2014, 53, 9679–9691

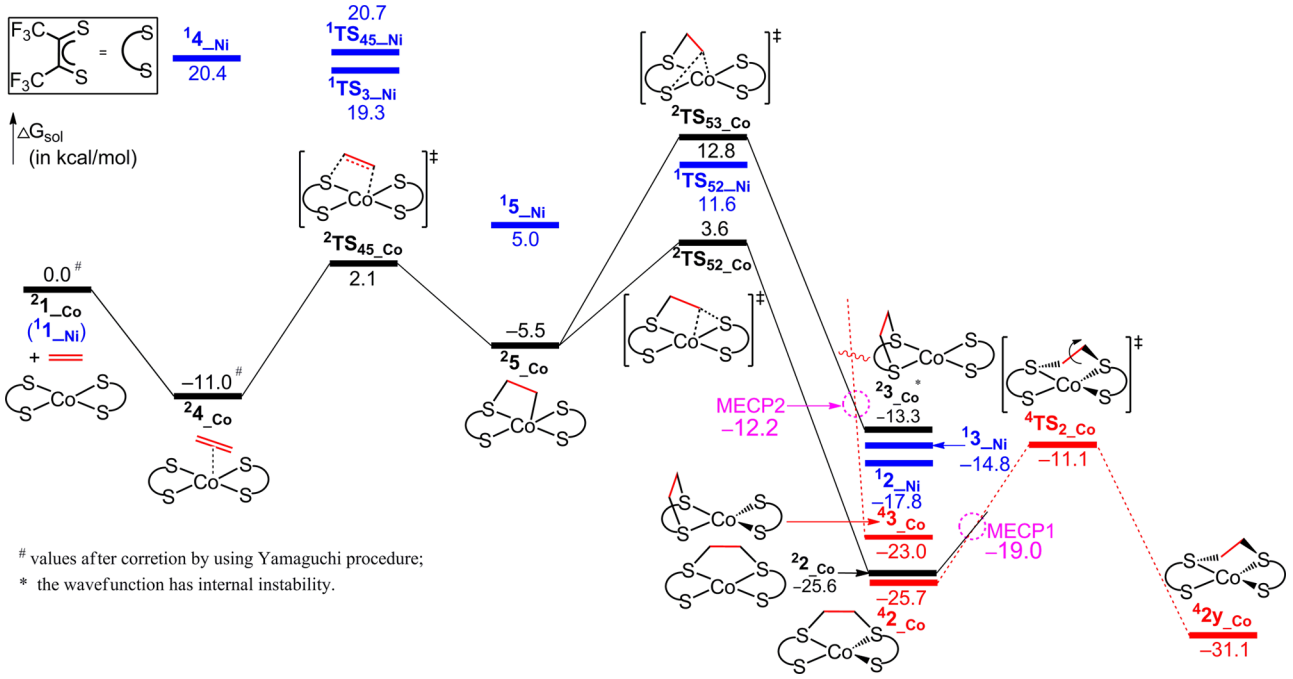

Figure 5. Calculated energy surfaces for the reaction of $\mathbf{1}_{Co}$ with ethylene via the most favorable pathways to form the intraligand and interligand adducts. Solid and dotted surfaces are the doublet and quartet state, respectively. Values in blue are the results for the nickel complex. Energies in kcal/mol are the free energy in solvent.

activation barrier of 13.1 kcal/mol relative to $^{2}\mathbf{4}_{Co}$. The atomic spin densities of $^{2}\mathbf{5}_{Co}$ are localized between the Co and two S atoms of the ligand without ethylene. $^{2}\mathbf{5}_{Co}$ can isomerize into the cis-interligand adduct $^{2}\mathbf{2}_{Co}$ through $^{2}\mathbf{TS}_{52\_Co}$ or into the intraligand adduct $^{2}\mathbf{3}_{Co}$ through $^{2}\mathbf{TS}_{53\_Co}$. The barriers for $^{2}\mathbf{TS}_{52\_Co}$ and $^{2}\mathbf{TS}_{53\_Co}$ are 9.1 and 18.3 kcal/mol, respectively, relative to $^{2}\mathbf{5}_{Co}$, implying that the indirect pathway favors the formation of the cis-interligand adduct $^{2}\mathbf{2}_{Co}$. Optimized geometries of $^{2}\mathbf{TS}_{52\_Co}$ and $^{2}\mathbf{TS}_{53\_Co}$ are consistent with their isomerization modes corresponding to breaking the Co−C bond and forming the C−S bond. The atomic spin densities on them are mainly on the Co atoms.

Comparisons of the two pathways in Figure 1 show that the indirect pathway is kinetically more favorable than the direct pathway, with the rate-determining barriers at 14.6 kcal/mol on the former and at 16.1 kcal/mol at the latter pathway. Along the favorable indirect pathway, the rate-determining barrier, $^{2}\mathbf{TS}_{52\_Co}$, for the formation of the cis-interligand adduct $^{2}\mathbf{2}_{Co}$ is lower than that, $^{2}\mathbf{TS}_{53\_Co}$, for the formation of the intraligand adduct $^{2}\mathbf{3}_{Co}$ by 9.2 kcal/mol. In addition, $^{2}\mathbf{2}_{Co}$ is more stable than $^{2}\mathbf{3}_{Co}$ by 12.3 kcal/mol. Thus, the kinetically and thermodynamically more favorable formation of the cis-interligand adduct on the doublet surfaces indicates that $^{2}\mathbf{1}_{Co}$ is an alternative catalyst that can avoid the decomposition issues of the nickel one. However, the reaction pathways on the quartet surfaces, which are close in energy, could compete with this pathway and alter this prediction (see below).

The direct and indirect pathways for the reaction of $^{4}\mathbf{1}_{Co}$ with ethylene on the quartet state surfaces are shown in Figure 3. Optimized geometries of selected intermediates and transition states are illustrated in Figure 4. Figure 3 shows that rather than the expected single transition state for the direct reaction to the twisted intermediate $^{4}\mathbf{2y}_{Co}$, there appears to be two successive (stepwise) transition states, namely, $^{4}\mathbf{TS}_{2y\_Co\_A}$ and $^{4}\mathbf{TS}_{2y\_Co\_B}$, at 15.8 and 9.4 kcal/mol relative to the separate $^{4}\mathbf{1}_{Co}$ and ethylene. In this reaction, each transition state corresponds to the formation of one C−S bond. It is worth noting that the energy of the intermediate $^{4}\mathbf{2y}_{Co\_int}$ in Figure 3 is obtained from a single point calculation based on the structure with converged forces but not distances. Full optimizations of $^{4}\mathbf{2y}_{Co\_int}$ repeatedly converge to the product $^{4}\mathbf{2y}_{Co}$; thus, the energy surface around $^{4}\mathbf{2y}_{Co\_int}$ is very flat, close to the second transition state $^{4}\mathbf{TS}_{2y\_Co\_B}$. Although $^{4}\mathbf{2y}_{Co}$ can isomerize into the cis-interligand adduct $^{4}\mathbf{2}_{Co}$ by overcoming a barrier of 20.0 kcal/mol, this process is thermodynamically unfavorable because $^{4}\mathbf{2}_{Co}$ is less stable than $^{4}\mathbf{2y}_{Co}$ by 5.4 kcal/mol. The formation of the intraligand adduct $^{4}\mathbf{3}_{Co}$ is also a stepwise process via two transition states $^{4}\mathbf{TS}_{3\_Co\_A}$ and $^{4}\mathbf{TS}_{3\_Co\_B}$. Here, it is clearer that the two C−S bonds are formed in two separate steps, with a fully converged intermediate, $^{4}\mathbf{3}_{Co\_int}$. A crossing between the two pathways, from $^{4}\mathbf{3}_{Co\_int}$ to $^{4}\mathbf{TS}_{2y\_Co\_B}$, may be possible, avoiding the high barrier of $^{4}\mathbf{TS}_{3\_Co\_B}$, but this crossing was not located, and the indirect pathway appears to be more favorable (see below). The electronic structure of $^{4}\mathbf{1}_{Co}$ shows two delocalized dithiolene ligands with the atomic spin densities for the Co and S atoms at 1.271 and 0.333, respectively, that is, the high-spin version of $^{2}\mathbf{1}_{Co}$. The delocalized character of the dithiolene ligands disappears in the ethylene adducts $^{4}\mathbf{2y}_{Co}$, $^{4}\mathbf{2}_{Co}$, and $^{4}\mathbf{3}_{Co}$, which have the atomic spin densities for the Co atoms of ∼2.5. Optimizations of the intraligand adduct $^{4}\mathbf{3}_{Co}$ with initial planar structure repeatedly converge to the tetrahedral geometry.

Along the indirect pathway, the first intermediate, $^{4}\mathbf{4}_{Co}$, at −2.2 kcal/mol relative to the separate $^{4}\mathbf{1}_{Co}$ and ethylene, is less stable than $^{2}\mathbf{4}_{Co}$ by 8.8 kcal/mol. Consistent with their relative stability, the two Co−C distances in the optimized geometry of $^{4}\mathbf{4}_{Co}$ are longer than those in $^{2}\mathbf{4}_{Co}$ by 0.404 and 0.375 Å, respectively. The barrier for $^{4}\mathbf{TS}_{45\_Co}$ corresponding to ethylene adding across the Co−S bond is 14.5 kcal/mol above $^{4}\mathbf{4}_{Co}$. Although the next intermediate, $^{4}\mathbf{5}_{Co}$, is unstable by 8.7 kcal/

dx.doi.org/10.1021/ic5011538 | Inorg. Chem. 2014, 53, 9679−9691

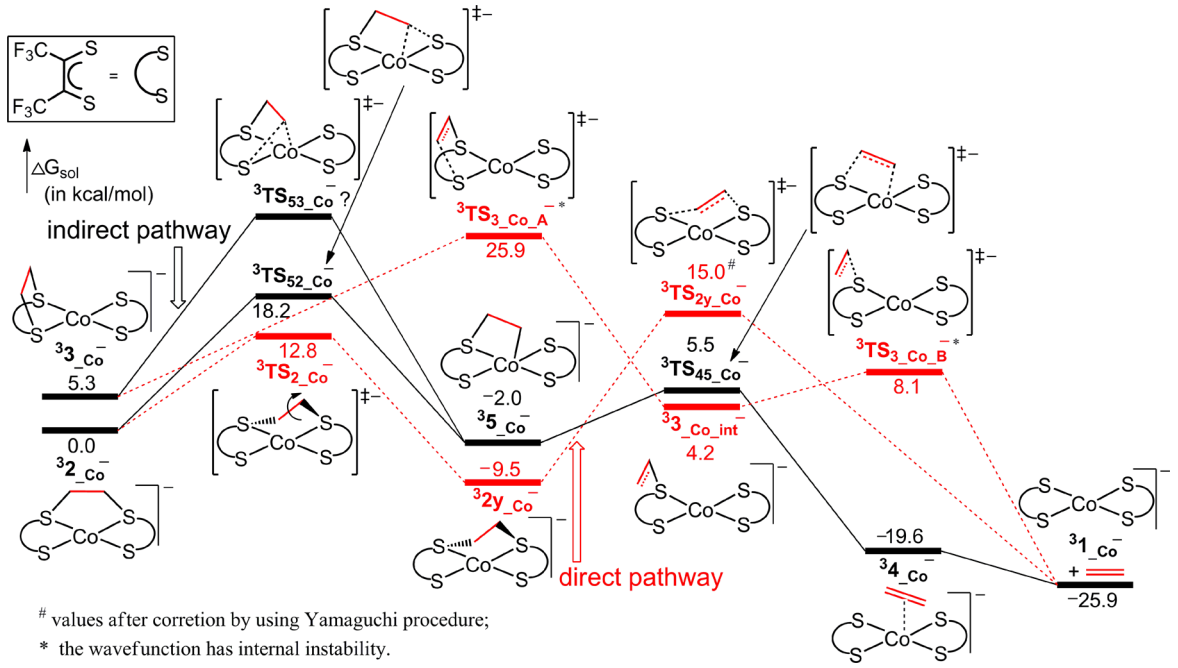

Figure 6. Calculated energy surfaces for the release of ethylene from the reduced adducts $^{3}\mathbf{2}_{Co}^{-}$ and $^{3}\mathbf{3}_{Co}^{-}$, through the direct pathway (dotted lines) or the indirect pathway (solid lines). Energies in kcal/mol are the free energy in solvent.

mol relative to $^{4}\mathbf{4}_{Co}$, it can easily isomerize into the cis-interligand adduct $^{4}\mathbf{2}_{Co}$ through $^{4}\mathbf{TS}_{52\_Co}$, while the change from transition state ($^{4}\mathbf{TS}_{53\_Co}$) to intraligand adduct $^{4}\mathbf{3}_{Co}$ is less favorable by 8.5 kcal/mol. Overall the most favorable reaction of $^{4}\mathbf{4}_{Co}$ leads to the cis-interligand adduct $^{4}\mathbf{2}_{Co}$. Optimized geometries of $^{4}\mathbf{TS}_{52\_Co}$ and $^{4}\mathbf{TS}_{53\_Co}$ in Figure 4 are consistent with the isomerization transition states.

Comparisons of the pathways in Figure 3 show that the formation of both interligand adducts $^{4}\mathbf{2y}_{Co}$ and $^{4}\mathbf{2}_{Co}$ favors the indirect pathway over the rate-determining barrier of $^{4}\mathbf{TS}_{45\_Co}$. Interestingly, the most stable of these interligand adducts is the twisted one, $^{4}\mathbf{2y}_{Co}$, whose most favorable route is via $^{4}\mathbf{2}_{Co}$, while the formation of the intraligand adduct $^{4}\mathbf{3}_{Co}$ prefers the direct pathway. The rate-determining pathway for these adducts, $^{4}\mathbf{2y}_{Co}$ and $^{4}\mathbf{2}_{Co}$, is 2.3 kcal/mol more favorable than that for the formation of $^{4}\mathbf{3}_{Co}$. Therefore, the reaction of $^{4}\mathbf{1}_{Co}$ with ethylene on the quartet state surfaces prefers to form the interligand adduct rather than form the intraligand adduct, both kinetically and thermodynamically.

Figure 5 shows the energy surfaces for the reaction of $\mathbf{1}_{Co}$ with ethylene to form the interligand and intraligand adducts by following the most favorable pathway among all the pathways in Figures 1 and 3. The reaction begins on the doublet surface by following the indirect pathway (solid lines), generating the cis-interligand adduct $^{2}\mathbf{2}_{Co}$. $^{2}\mathbf{2}_{Co}$ and its quartet state complex $^{4}\mathbf{2}_{Co}$ have nearly the same energy (with the ωB97X-D functional), while the twisted product $^{4}\mathbf{2y}_{Co}$ is the most stable adduct, at 5.5 kcal/mol below $^{2}\mathbf{2}_{Co}$. According to these calculations, $^{2}\mathbf{2}_{Co}$ would be formed first, but could then cross onto the quartet state at the minimum energy crossing point (MECP1) with a barrier of 6.6 kcal/mol to generate $^{4}\mathbf{2}_{Co}$ or $^{4}\mathbf{2y}_{Co}$. When the intraligand adduct $^{2}\mathbf{3}_{Co}$ is formed, it can also transfer onto its quartet state to complex $^{4}\mathbf{3}_{Co}$ by overcoming a minimum energy crossing point (MECP2), only 1.1 kcal/mol higher than the energy of $^{2}\mathbf{3}_{Co}$.

In comparison with the nickel system (results in blue), the neutral cobalt compex $\mathbf{1}_{Co}$ performs better at binding ethylene, favoring the indirect pathway to selectively form the interligand adduct (avoiding the decomposition issues). In contrast, $\mathbf{1}_{Ni}$ does not coordinate ethylene to Ni because of the "four e^{-} repulsive interactions," and it favors the direct pathway to form the intraligand adduct, which decomposes. Because $\mathbf{1}_{Co}$ binds ethylene so strongly, it proceeds via the indirect pathway, which prefers forming the interligand adduct to forming the intraligand adduct. This strong preference, which is also seen in the indirect pathway for $\mathbf{1}_{Ni}$, arises because the rate-determining isomerization transition state to the interligand adduct is lower than that to the intraligand adduct. This energetic difference can be explained by comparing the optimized geometries of $^{2}\mathbf{TS}_{52\_Co}$ and $^{2}\mathbf{TS}_{53\_Co}$ (Figure 2) or $^{4}\mathbf{TS}_{52\_Co}$ and $^{4}\mathbf{TS}_{53\_Co}$ (Figure 4). In both comparisons, the new C−S bonds that are forming have nearly identical distances for the intra- and interligand transition states; however, the Co−C bonds that are breaking are much shorter in $^{2}\mathbf{TS}_{52\_Co}$ and $^{4}\mathbf{TS}_{52\_Co}$ than those in $^{2}\mathbf{TS}_{53\_Co}$ and $^{4}\mathbf{TS}_{53\_Co}$. Thus, migration from the Co−S ethylene adduct $^{2}\mathbf{5}_{Co}$ or $^{4}\mathbf{5}_{Co}$ to the interligand product preserves more Co−C bonding while making the new C−S bond. Therefore, $^{2}\mathbf{TS}_{53\_Co}$ (or $^{4}\mathbf{TS}_{53\_Co}$) is higher in energy than $^{2}\mathbf{TS}_{52\_Co}$ (or $^{4}\mathbf{TS}_{52\_Co}$). Knowledge of this difference provides us a route to additional catalyst improvement by making modifications to facilitate the indirect pathway. Here, changing from Ni to Co improved the performance because the Co atom with its unpaired electron(s) (d^{7} rather that d^{8} as in Ni) coordinates with ethylene favorably. In the previously described Ni system, addition of the anion $\mathbf{1}_{Ni}^{-}$, with formation of the dimer, released the four e^{-} repulsive interactions and lowered the barriers for the formation of an important intermediate $^{1}\mathbf{5}_{Ni}$ in the indirect pathway.

As mentioned above, the ωB97X-D functional underestimates the HS−LS gaps, favoring the HS state by at least 6 kcal/mol for the Ni(edt)$_2$ system, where the spin change

dx.doi.org/10.1021/ic5011538 | Inorg. Chem. 2014, 53, 9679−9691

occurs on the Ni atom. Comparisons of $^2\mathbf{2}_{Co}$ (Figure 2) and $^4\mathbf{2}_{Co}$, $^4\mathbf{2y}_{Co}$ (Figure 4) show that the spin change in these processes also occurs on the Co atom. Therefore, after consideration of the ωB97X-D underestimation of the HS−LS gaps, $^2\mathbf{2}_{Co}$ should be much more stable than $^4\mathbf{2}_{Co}$ and also more stable than $^4\mathbf{2y}_{Co}$ by at least 0.5 kcal/mol. Furthermore, the interligand adduct $^2\mathbf{2}_{Co}$ is calculated to be more stable by 2.6 kcal/mol than the intraligand adduct $^4\mathbf{3}_{Co}$; the difference should be larger when considering the underestimation of HS−LS gaps. $^2\mathbf{TS}_{52\_Co}$ is also lower than $^2\mathbf{TS}_{53\_Co}$ by 9.2 kcal/mol. Therefore, the formation of the interligand adduct in the neutral Co system is more favorable than the formation of the intraligand adduct both thermodynamically and kinetically.

Although it is clear that formation of the interligand adduct $^2\mathbf{2}_{Co}$ is quite favorable, to perform catalysis ethylene must be released upon reduction of $^2\mathbf{2}_{Co}$. Release of ethylene from the anionic adducts on both the singlet and triplet surfaces was considered, and the triplet surface was found to be more favorable. The stability calculations show that nearly all the singlet-state intermediates and transition states have RHF > UHF unstable wave functions (see Supporting Information for further details about the singlet process). Figure 6 shows the triplet-state surface for the release of ethylene from the anionic ethylene adducts $^3\mathbf{2}_{Co}^-$, $^3\mathbf{2y}_{Co}^-$, and $^3\mathbf{3}_{Co}^-$. $^3\mathbf{2}_{Co}^-$ can release ethylene via the indirect pathway by crossing a rate-determining transition state $^3\mathbf{TS}_{52\_Co}^-$ at 18.2 kcal/mol. This process is thermodynamically favorable by releasing 25.9 kcal/mol of energy. Alternatively, $^3\mathbf{2}_{Co}^-$ isomerizes to $^3\mathbf{2y}_{Co}^-$ with a barrier of only 12.8 kcal/mol, from which ethylene can be released via the direct pathway by overcoming a barrier of 24.5 kcal/mol for $^3\mathbf{TS}_{2y\_Co}^-$, which is higher than the indirect transition state $^3\mathbf{TS}_{52\_Co}^-$ by 6.3 kcal/mol. Furthermore, even though the formation of the intraligand adduct $^3\mathbf{3}_{Co}$ is unfavorable, upon reduction it also would release ethylene, through transition states $^3\mathbf{TS}_{3\_Co\_A}^-$ and $^3\mathbf{TS}_{3\_Co\_B}^-$ via the direct pathway (calculations of indirect transition state $^3\mathbf{TS}_{53\_Co}^-$ repeatedly converge to either $^3\mathbf{TS}_{3\_Co\_A}^-$ or $^3\mathbf{TS}_{3\_Co\_B}^-$). Therefore, ethylene can be released from the reduced interligand adduct $^3\mathbf{2y}_{Co}^-$ (and the reduced intraligand adduct, $^3\mathbf{3}_{Co}^-$) both kinetically and thermodynamically, although the barrier is somewhat large.

The catalytic reaction involves two electrochemical processes of the reduction of the ethylene adducts $^2\mathbf{2}_{Co}$ or $^4\mathbf{2y}_{Co}$ and the oxidation of the anion $^3\mathbf{1}_{Co}^-$. Theoretical predictions of the standard redox potentials of complexes in solution have been reported on the basis of the Born−Haber cycle.[25] The same method was used here to calculate the redox potentials for the corresponding complexes (Table 3). The calculated E^0 for the half reaction $^1\mathbf{1}_{Ni} + e^- \rightarrow {}^1\mathbf{1}_{Ni}^-$ is close to the experimentally reported value for the $Ni(mnt)_2 + e^- \rightarrow [Ni(mnt)_2]^-$ half reaction.[4] As shown in Table 3, the reduction of both $^2\mathbf{2}_{Co}$ and $^4\mathbf{2y}_{Co}$ (the process to release ethylene) is more difficult than that of $^1\mathbf{2}_{Ni}$. Likewise, the oxidation of $^3\mathbf{1}_{Co}^-$ (to regenerate the neutral complex to bind ethylene) is also more difficult than the oxidation of $^1\mathbf{1}_{Ni}^-$. Therefore, although the neutral cobalt complex $\mathbf{1}_{Co}$ is predicted to be a reasonable alternative catalyst for ethylene purification, the electrochemical steps cost more energy than those for the Ni system.

A series of cobalt dithiolene complexes were reported to be exceptionally active for the catalytic reduction of protons in aqueous solvent mixtures to produce hydrogen.[26] The electrochemical reaction pathway was studied computationally by calculating the reduction potentials for hydrogen evolution.[27] In the experiment study, a complex, $[Co(mnt)_2]^-$ (mnt = $S_2C_2(CN)_2$), was characterized structurally in the solid state as the dimer $[(Co(mnt)_2)_2]^{2-}$;[26] in agreement with this observation calculations predict that this dimer is more stable than the monoanions by 12.7 kcal/mol in solution (see Supporting Information). Calculations on the formation of dimers from $^2\mathbf{1}_{Co}$ or $^3\mathbf{1}_{Co}^-$ show that there is a stable dimer of $^2\mathbf{1}_{Co}$, but since the ethylene adducts of $^2\mathbf{1}_{Co}$ are much more stable thermodynamically, this dimer will dissociate under ethylene. Dimers of $^3\mathbf{1}_{Co}^-$ are predicted to be less stable than their monoanions by ∼30 kcal/mol (see Supporting Information); from the structure and electronic energies it appears that the $-CF_3$ substituent groups play an important role in preventing the dimerization of $^3\mathbf{1}_{Co}^-$, while the less sterically demanding −CN group allows the formation of the experimentally observed dimer $[Co(mnt)_2]_2^{2-}$.[26]

Table 3. Calculated Reduction Potentials with Respect to Fc/Fc^+

half reactions	E^0 (V)
$Ni(mnt)_2 + e^- \rightarrow [Ni(mnt)_2]^-$	0.69[a]
$^1\mathbf{1}_{Ni} + e^- \rightarrow {}^1\mathbf{1}_{Ni}^-$	0.76
$^1\mathbf{2}_{Ni} + e^- \rightarrow {}^1\mathbf{2}_{Ni}^-$	−0.83
$^2\mathbf{1}_{Co} + e^- \rightarrow {}^3\mathbf{1}_{Co}^-$	1.15
$^2\mathbf{2}_{Co} + e^- \rightarrow {}^3\mathbf{2}_{Co}^-$	−1.10
$^4\mathbf{2y}_{Co} + e^- \rightarrow {}^3\mathbf{2y}_{Co}^-$	−0.93
$^1\mathbf{1}_{Cu}^- + e^- \rightarrow {}^2\mathbf{1}_{Cu}^{2-}$	−1.00
$^1\mathbf{2y}_{Cu}^- + e^- \rightarrow {}^2\mathbf{2y}_{Cu}^{2-}$	−3.17

[a]The experimental value that is reported in ref 4; mnt = $S_2C_2(CN)_2$

3.3. Transition States for the Reaction of Copper Bis(dithiolene) Complexes with Ethylene. The thermodynamics results in Section 3.1 show that the neutral copper complex $^2\mathbf{1}_{Cu}$ might be an alternative Cu catalyst if the favorably formed intraligand adduct $^2\mathbf{3}_{Cu}$ does not decompose. The decomposition of $^2\mathbf{3}_{Cu}$ is compared to the decomposition of $^1\mathbf{3}_{Ni}$, which experimentally decomposes into dihydrodithiin (**DHD**) and metal dimer as model for decomposition (**MD**)[7,8] in Figure 7. The $^1\mathbf{3}_{Ni}$ decomposes by dissociating into ^{1}**DHD** and ^{3}**MM** (metal monomer) intermediates 18.2 kcal/mol less stable, then stabilizing the ^{3}**MM** by forming a dimer. The products, $(1/2)^3$**MD** and ^{1}**DHD**, in this simplified decomposition model are predicted to be higher than $^1\mathbf{3}_{Ni}$ by only 4.4 kcal/mol (Figure 7A). A similar decomposition model for $^2\mathbf{3}_{Cu}$ was determined and, as shown in Figure 7B, is much more favorable than the experimentally known decomposition for the Ni complex. Thus, the neutral copper complex $^2\mathbf{1}_{Cu}$ is excluded as an alternative catalyst.

From the results in Section 3.1, the anionic copper complex $^1\mathbf{1}_{Cu}^-$ might also be an alternative Cu catalyst, as the reaction is close to zero free energy change. The most favorable computed energy surfaces for the reaction of $\mathbf{1}_{Cu}^-$ with ethylene are shown in Figure 8 (unfavorable indirect pathways are given in the Supporting Information). The direct reaction occurs concertedly on the singlet-state surface, while it occurs stepwisely on the triplet-state surface. Both the interligand and intraligand ethylene adducts favor the singlet spin state, $^1\mathbf{2y}_{Cu}^-$ and $^1\mathbf{3}_{Cu}^-$. The more stable interligand adduct $^1\mathbf{2y}_{Cu}^-$ is −9.5 kcal/mol relative to the separate $^1\mathbf{1}_{Cu}^-$ and ethylene and is predicted to form over a barrier of 36.6 kcal/mol, $^1\mathbf{TS}_{2y\_Cu}^-$. Although $^3\mathbf{TS}_{2y\_Cu\_A}^-$ is a lower energy transition

dx.doi.org/10.1021/ic5011538 | Inorg. Chem. 2014, 53, 9679−9691

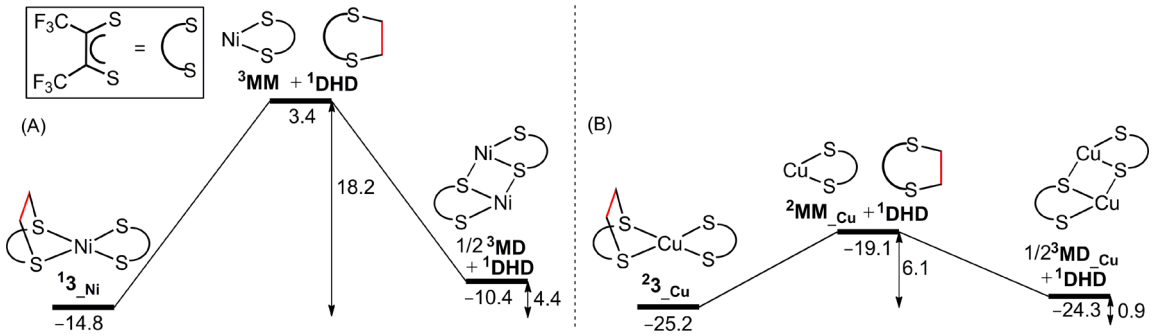

Figure 7. Calculated energy surfaces for the model decomposition process of $^{1}\mathbf{3}_{\_Ni}$ (A) and $^{2}\mathbf{3}_{\_Cu}$ (B). The species reported are their most stable conformations. Energies in kcal/mol are free energies in solvent.

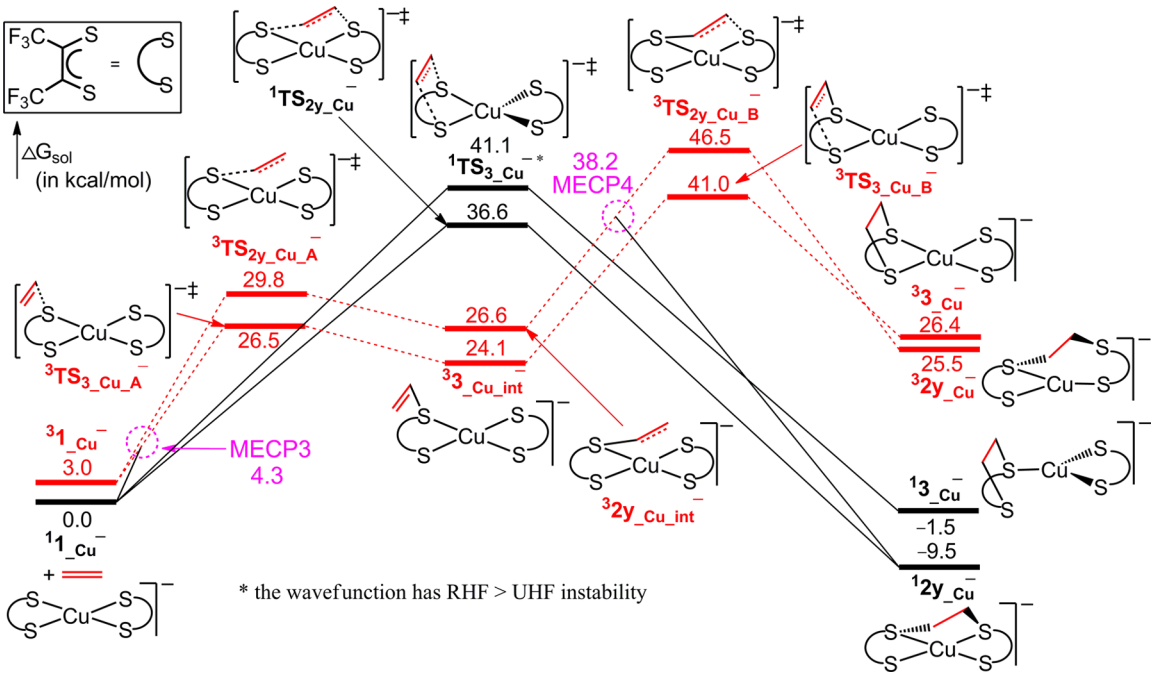

Figure 8. Calculated energy surfaces for the reaction of $\mathbf{1}_{\_Cu}^{-}$ with ethylene via the direct pathway. Surfaces on the singlet spin state and triplet spin state are marked in solid and dotted lines, respectively. Energies in kcal/mol are the free energy in solvent.

state, later transition states on this reaction surface, $^{3}\mathbf{TS}_{\mathbf{2y\_Cu\_B}}^{-}$ and MECP4, are higher in energy than that for $^{1}\mathbf{TS}_{\mathbf{2y\_Cu}}^{-}$. The intraligand adduct $^{1}\mathbf{3}_{\_Cu}^{-}$ is predicted to form concertedly over a barrier of 41.1 kcal/mol, $^{1}\mathbf{TS}_{\mathbf{3\_Cu}}^{-}$. Alternatively, it can be formed on the triplet surface as $^{1}\mathbf{1}_{\_Cu}^{-}$ first transfers onto the $^{3}\mathbf{1}_{\_Cu}^{-}$ surface via MECP3 and then proceeds through two stepwise transition states, $^{3}\mathbf{TS}_{\mathbf{3\_Cu\_A}}^{-}$ and $^{3}\mathbf{TS}_{\mathbf{3\_Cu\_B}}^{-}$, to form the ethylene adduct $^{3}\mathbf{3}_{\_Cu}^{-}$ that can finally transfer back onto $^{1}\mathbf{3}_{\_Cu}^{-}$ surface. The possibility for this latter crossing between $^{3}\mathbf{3}_{\_Cu\_int}^{-}$ and $^{1}\mathbf{3}_{\_Cu}^{-}$ was searched and computed to be even higher than $^{3}\mathbf{TS}_{\mathbf{3\_Cu\_B}}^{-}$. The rate-determining barriers for the formation of either $^{3}\mathbf{3}_{\_Cu}^{-}$ or $^{1}\mathbf{3}_{\_Cu}^{-}$, $^{3}\mathbf{TS}_{\mathbf{3\_Cu\_B}}^{-}$ (41.0 kcal/mol), and $^{1}\mathbf{TS}_{\mathbf{3\_Cu}}^{-}$ (41.1 kcal/mol) are comparable, but they are higher than that for the formation of the interligand adduct $^{1}\mathbf{2y}_{\_Cu}^{-}$, $^{1}\mathbf{TS}_{\mathbf{2y\_Cu}}^{-}$ (36.6 kcal/mol). Since the cis-interligand adduct $^{1}\mathbf{2}_{\_Cu}^{-}$ is less stable than $^{1}\mathbf{2y}_{\_Cu}^{-}$ by 6.2 kcal/mol, the isomerization of $^{1}\mathbf{2y}_{\_Cu}^{-}$ to $^{1}\mathbf{2}_{\_Cu}^{-}$ was not shown in Figure 8. The optimized geometry of $^{1}\mathbf{3}_{\_Cu}^{-}$ (see the Supporting Information) has only three sulfur atoms coordinate with the copper atom, and $^{1}\mathbf{3}_{\_Cu}^{-}$ is less stable than $^{1}\mathbf{2y}_{\_Cu}^{-}$ by 8.0 kcal/mol. Therefore, the reaction of $^{1}\mathbf{1}_{\_Cu}^{-}$ with ethylene favors the formation of the interligand adduct $^{1}\mathbf{2y}_{\_Cu}^{-}$ both kinetically and thermodynamically. However, the barrier is rather unfavorable, and $^{1}\mathbf{2y}_{\_Cu}^{-}$ is not very stable; therefore, $^{1}\mathbf{1}_{\_Cu}^{-}$ does not appear to be a good catalytic candidate, although some modifications of it might make it more viable.

When $^{1}\mathbf{2y}_{\_Cu}^{-}$ is reduced to $^{2}\mathbf{2y}_{\_Cu}^{2-}$, it releases ethylene easily (see the Supporting Information). Although the $^{4}\mathbf{2y}_{\_Cu}^{2-}$ also releases ethylene easily, its entire energy surface is much less stable. The calculated E^{0} values in Table 3 show that the oxidation of $^{2}\mathbf{1}_{\_Cu}^{2-}$ occurs easily, while the reduction of $^{1}\mathbf{2y}_{\_Cu}^{-}$ is more difficult than the corresponding reduction in the experimentally reported nickel system.

4. CONCLUSION

In summary, density functional theory, calibrated to coupled cluster theory, has been used to predict alternative catalysts $M(S_2C_2(CF_3)_2)_2$ (M = Co and Cu) for olefin purification. Inspired by the catalytic nickel system that possesses a reversible one-electron transfer series $[Ni(S_2C_2(CF_3)_2)_2]$ ($\mathbf{1}_{\_Ni}$) ↔ $[Ni(S_2C_2(CF_3)_2)_2]^{-}$ ($\mathbf{1}_{\_Ni}^{-}$) ↔ $[Ni(S_2C_2(CF_3)_2)_2]^{2-}$ ($\mathbf{1}_{\_Ni}^{2-}$), various cobalt and copper complexes that are

dx.doi.org/10.1021/ic5011538 | Inorg. Chem. 2014, 53, 9679−9691

isoelectronic or isocharged to the three forms of the nickel complexes were examined (Scheme 4). Both thermodynamics and kinetics (transition state) results show that the neutral cobalt complex $\mathbf{1}_{Co}$ is an alternative catalyst that is predicted to perform better than $\mathbf{1}_{Ni}$, because the reaction prefers to form the interligand adduct rather than the intraligand adduct both thermodynamically and kinetically via the indirect pathway, effectively blocking the decomposition route. The nickel system avoids decomposition only by having a high enough concentration of the anion to make dimer formation predominate, a situation that opens the low-energy indirect route. In contrast, no anion is required in the cobalt system. The favorability of the Co atom coordinating to ethylene facilitates the indirect pathway, which in this case prefers to form the interligand adduct, $^{4}\mathbf{2y}_{Co}$. When $^{4}\mathbf{2y}_{Co}$ is reduced to $^{3}\mathbf{2y}_{Co}^{-}$, it releases ethylene to generate $^{3}\mathbf{1}_{Co}^{-}$, which then can be oxidized to regenerate the catalyst. The electrochemical processes for the reduction of $^{4}\mathbf{2y}_{Co}$ and the oxidization of $^{3}\mathbf{1}_{Co}^{-}$ are computed to be at reasonable values that might be improved by ligand modifications. The thermodynamic and kinetic (transition state) results for the copper complexes show that the anionic copper complex $\mathbf{1}_{Cu}^{-}$ might be an alternative catalyst, but it has quite high barriers. However, the nearly neutral thermodynamics of the reaction of $\mathbf{1}_{Cu}^{-}$ with ethylene indicates that it might be possible to design catalysts that can perform thermally if the barriers can be reduced by modifying the dithiolene ligands on $\mathbf{1}_{Cu}^{-}$. These theoretical studies provide some guidance to the design of new catalysts to examine experimentally.

■ ASSOCIATED CONTENT

Ⓢ Supporting Information

Calculated energies together with $\langle S^2 \rangle$ for the species before corrections by using Yamaguchi procedure; comparisons between optimizing in gas phase and in solvent for the one-negative-charged species; results for the CCSD(T) calculations for the HS−LS gaps; molecular orbital results; pathways for the release of ethylene from $^{1}\mathbf{2}_{Co}^{-}$ and $^{1}\mathbf{3}_{Co}^{-}$; possible dimers of $^{2}\mathbf{1}_{Co}$ or $^{3}\mathbf{1}_{Co}^{-}$; indirect pathways for the reaction of $\mathbf{1}_{Cu}$ and ethylene; pathways for the release of ethylene from $^{2}\mathbf{2y}_{Cu}^{2-}$ and $^{4}\mathbf{2y}_{Cu}^{2-}$; optimized geometries of stationary points involved in the figures but not shown in the text; and the total energies and Cartesian coordinates of the structures involved in this study. This material is available free of charge via the Internet at http://pubs.acs.org.

■ AUTHOR INFORMATION

Corresponding Authors

*E-mail: mbhall@tamu.edu. (M.B.H.)

*E-mail: ed.brothers@qatar.tamu.edu. (E.N.B.)

Notes

The authors declare no competing financial interest.

■ ACKNOWLEDGMENTS

We acknowledge finanicial support from the Qatar National Research Fund under NPRP Grant No. 05-318-1-063. Computer time was provided by the TAMU Supercomputer Facility. We thank Z. Xu for the discussions on some technical skills.

■ REFERENCES

(1) (a) National Research Council. *Separation and Purificaton: Critical Needs and Opportunities;* National Academy Press: Washington, DC, 1987. (b) Sundaram, K. M.; Shreehan, M. M.; Olszewski, E. F. *Kirk-Othmer Encyclopedia of Chemical Technology;* Wiley: New York, 4th ed, 1995; pp 877−915.

(2) (a) Grantom, R. L.; Royer, D. J. In *Ullmann's Encyclopedia of Industrial Chemistry,* 5th ed.; VCH: New York, 1987; pp 45−93. (b) Ladwig, P. K. Chapter 3.1. In *Handbook of Petroleum Refining Processes;* Meyers, R. A., Ed.; Mc Graw-Hill: New York, 2th ed.; 1997.

(3) Suzuki, T.; Noble, R. D.; Koval, C. A. *Inorg. Chem.* **1997**, *36*, 136.

(4) Wang, K.; Stiefel, E. I. *Science* **2001**, *291*, 106.

(5) (a) Wing, R. M.; Tustin, G. W.; Okamura, W. H. *J. Am. Chem. Soc.* **1970**, *92*, 1935. (b) Harrison, D.; Nguyen, N.; Lough, A.; Fekl, U. *J. Am. Chem. Soc.* **2006**, *128*, 11026.

(6) Fan, Y.; Hall, M. *J. Am. Chem. Soc.* **2002**, *124*, 12076.

(7) Dang, L.; Shibl, M.; Yang, X.; Alak, A.; Harrison, D.; Fekl, U.; Brothers, E.; Hall, M. *J. Am. Chem. Soc.* **2012**, *134*, 4481.

(8) Dang, L.; Shibl, M.; Yang, X.; Harrison, D.; Alak, A.; Lough, A.; Fekl, U.; Brothers, E.; Hall, M. *Inorg. Chem.* **2013**, *52*, 3711.

(9) Frisch, M. J.; Trucks, G. W.; Schlegel, H. B.; Scuseria, G. E.; Robb, M. A.; Cheeseman, J. R.; Scalmani, G.; Barone, V.; Mennucci, B.; Petersson, G. A.; Nakatsuji, H.; Caricato, M.; Li, X.; Hratchian, H. P.; Izmaylov, A. F.; Bloino, J.; Zheng, G.; Sonnenberg, J. L.; Hada, M.; Ehara, M.; Toyota, K.; Fukuda, R.; Hasegawa, J.; Ishida, M.; Nakajima, T.; Honda, Y.; Kitao, O.; Nakai, H.; Vreven, T.; Montgomery, J. A.; Jr., Peralta, J. E.; Ogliaro, F.; Bearpark, M.; Heyd, J. J.; Brothers, E.; Kudin, K. N.; Staroverov, V. N.; Kobayashi, R.; Normand, J.; Raghavachari, K.; Rendell, A.; Burant, J. C.; Iyengar, S. S.; Tomasi, J.; Cossi, M.; Rega, N.; Millam, J. M.; Klene, M.; Knox, J. E.; Cross, J. B.; Bakken, V.; Adamo, C.; Jaramillo, J.; Gomperts, R.; Stratmann, R. E.; Yazyev, O.; Austin, A. J.; Cammi, R.; Pomelli, C.; Ochterski, J. W.; Martin, R. L.; Morokuma, K.; Zakrzewski, V. G.; Voth, G. A.; Salvador, P.; Dannenberg, J. J.; Dapprich, S.; Daniels, A. D.; Farkas, O.; Foresman, J. B.; Ortiz, J. V.; Cioslowski, J.; Fox, D. J. *Gaussian 09, Revision B.01;* Gaussian, Inc.: Wallingford, CT, 2010.

(10) Dang, L.; Yang, X.; Zhou, J.; Brothers, E.; Hall, M. *J. Phys. Chem. A* **2012**, *116*, 476.

(11) Chai, J.-D.; Head-Gordon, M. *Phys. Chem. Chem. Phys.* **2008**, *10*, 6615.

(12) (a) Hehre, W. J.; Ditchfie, R.; Pople, J. A. *J. Chem. Phys.* **1972**, *56*, 2257. (b) Francl, M. M.; Pietro, W. J.; Hehre, W. J.; Binkley, J. S.; Gordon, M. S.; Defrees, D. J.; Pople, J. A. *J. Chem. Phys.* **1982**, *77*, 3654. (c) Clark, T.; Chandrasekhar, J.; Spitznagel, G. W.; Schleyer, P. v. R. *J. Comput. Chem.* **1983**, *4*, 294.

(13) Fukui, K. *Acc. Chem. Res.* **1981**, *14*, 363.

(14) (a) Seeger, R.; Pople, J. A. *J. Chem. Phys.* **1977**, *66*, 3045. (b) Schlegel, H. B.; McDouall, J. J. W. In *Computationl Advances in Organic Chemistry;* Ögretir, C.; Csizmadia, I. G., Ed. Kluwer Academic: The Netherlands, 1991; pp 161−185. (c) Bauernschmitt, R.; Ahlrichs, R. *J. Chem. Phys.* **1996**, *104*, 9047.

(15) (a) Yamaguchi, K.; Jensen, F.; Dorigo, A.; Houk, K. N. *Chem. Phys. Lett.* **1988**, *149*, 537. (b) Soda, T.; Kitagawa, Y.; Onishi, T.; Takano, Y.; Shigeta, Y.; Nagao, H.; Yoshioka, Y.; Yamaguchi, K. *Chem. Phys. Lett.* **2000**, *319*, 223.

(16) Marenich, A. V.; Cramer, C. J.; Truhlar, D. G. *J. Phys. Chem. B* **2009**, *113*, 6378.

(17) Pitts, A. L.; Hall, M. B. *Inorg. Chem.* **2013**, *52*, 10387.

(18) Harvey, J.; Aschi, M.; Schwarz, H.; Koch, W. *Theor. Chem. Acc.* **1998**, *99*, 95.

(19) (a) Bursten, B. E.; Jensen, J. R.; Fenske, R. F. *J. Chem. Phys.* **1978**, *68*, 3320. (b) Hall, M. B.; Fenske, R. F. *Inorg. Chem.* **1972**, *11*, 768. (c) Webster, C. E.; Pérez, L. M.; Hall, M. B. *JIMP2, Version 091,* 2006 http://www.chem.tamu.edu/jimp2/index.html.

(20) Sugimori, A.; Akiyama, T.; Kajitani, M.; Sugiyama, T. *Bull. Chem. Soc. Jpn.* **1999**, *72*, 879.

(21) Muellerwesterhoff, U. T.; Herman, Z.; Kirchner, R.; Loew, G.; Mueller-Westerhoff, U.; Nazzal, A.; Zerner, M. *Inorg. Chem.* **1982**, *21*, 46.

(22) (a) Bachler, V.; Olbrich, G.; Neese, F.; Wieghardt, K. *Inorg. Chem.* **2002**, *41*, 4179. (b) Ray, K.; Weyhermuller, T.; Weyhermüller, T.; Neese, F.; Wieghardt, K. *Inorg. Chem.* **2005**, *44*, 5345.
(23) (a) Davison, A.; Edelstein, N.; Holm, R. H.; Maki, A. H. *J. Am. Chem. Soc.* **1963**, *85*, 2029. (b) Schrauze, G. N. *Acc. Chem. Res.* **1969**, *2*, 72.
(24) Shibl, M.; Dang, L.; Raju, R.; Hall, M.; Brothers, E. *Int. J. Quantum Chem.* **2013**, *113*, 1621.
(25) (a) Li, J.; Fisher, C.; Chen, J.; Bashford, D.; Noodleman, L. *Inorg. Chem.* **1996**, *35*, 4694. (b) Surawatanawong, P.; Tye, J.; Darensbourg, M.; Hall, M. *Dalton Trans.* **2010**, *39*, 3093.
(26) McNamara, W. R.; Han, Z.; Yin, C.-J.; Brennessel, W. W.; Holland, P. L.; Eisenberg, R. *Proc. Natl. Acad. Sci. U. S. A.* **2012**, *109*, 15594.
(27) Solis, B. H.; Hammes-Schiffer, S. *J. Am. Chem. Soc.* **2012**, *134*, 15253.